

BACHELOR THESIS



MOTION CONTROL OF IRONSPERM CLUSTERS IN A VASCULAR MODEL

Remco Braks

FACULTY OF ENGINEERING TECHNOLOGY – DEPARTMENT OF
BIOMECHANICAL ENGINEERING

EXAMINATION COMMITTEE

Dr. Islam S. M. Khalil
Prof. Dr. Sarthak Misra
Dr. Janset Dasedemir

DOCUMENT NUMBER

BE - 938

Motion control of IRONSperm clusters in a vascular model

R.J.M. Braks

July, 2023

Abstract

Biohybrid microrobots can possibly be used for *in vivo* targeted drug delivery since they can reach hard-to-reach places without invasive surgery. In this paper, the control of an IRONSperm biohybrid micro-robot inside of a vascular network is investigated. In order to achieve this, the vascular network was imaged. The centerline of a path throughout the phantom was acquired. This reconstruction is the foundation for the motion of the rotating magnet has to make in order to guide the rolling IRONSperm cluster through the vascular network. The locomotion parameters of the IRONSperm cluster, the rolling velocity and actuation distance, are determined. Because of the rolling locomotion, the cluster can only be controlled in one plane simultaneously. Because of this, an alternative way was used to guide the IRONSperm cluster in the third direction. By use of magnetic attraction, the IRONSperm cluster was transferred to the top of the vascular network, after which the attractive forces could handle the inclining parts of the vascular network. This principle was proven to be successful in a test setup. Due to mechanical limitations, the IRONSperm cluster could not be tested in the vascular network, however, the preliminary experiments conducted in this paper offer good prospects for navigation inside a vascular network.

1 Introduction

In the current world of healthcare and medicine, making treatments as minimally invasive as possible has become the norm. Research into minimally invasive ways to treat diseases has been going on since the 1900s [1], but it is a topic with great potential for the future. One way to decrease the invasiveness of current surgical procedures is to deliver the drug only to the place where the drug is needed, without harming the body in unnecessary

ways.

One of the ways to achieve controlled drug delivery is microrobots [2]. Due to their size, they have the ability to reach difficult places in the body. This size, however, limits the possibilities of built-in control mechanisms. This constraint leads to the need for remote actuation and control. Over the past years, magnetic actuation has proven to be a safe way to actuate magnetic microrobots in a surgical environment [3, 4].

Synthetic robots are the most common type of robot. However, it can be a challenge to reduce all the components of a synthetic robot (joints, drivers, executing mechanisms etc.) to a micrometre scale. Furthermore, *in vivo* applications of microrobots require the need for biocompatible materials. Stanton *et al.* proposed a solution to both challenges with the introduction of biohybrid microrobots [5, 6, 7]. Biohybrid microrobots consist partly of synthetic materials, combined with biological units. This yields a reduced concentration of synthetic materials in the body while maintaining volume and drug-loading capabilities.

In this research, the rolling motion control by means of magnetic actuation of the biohybrid microrobots, IRONSperm, inside confinement will be investigated. IRONSperm consists of bovine sperm cells, coated with iron nanoparticles. This fabrication is done by electrostatic self-assembly [8]. Since individual IRONSperm lack the speed to navigate through the bloodstream [9], IRONSperm clusters will be investigated.

2 Magnetic Torque on IRONSperm

2.1 IRONSperm cluster

There are many different configurations of IRONSperm [10]. When clustering the individual IRONSperm, the individual configurations and properties disappear. Previous research [8] has shown that IRONSperm clusters can be approximated as soft-magnet ellipsoids. When actuated by a rotating, permanent magnet, the clusters rotate accordingly.

2.2 Cluster formation

Starting with individual IRONSperm, these have to form clusters. IRONSperm entangles due to physical interactions, forming clusters. Afterwards, further accumulation of the IRONSperm clusters can be achieved by the use of an rotating external magnetic field. The possible heterogeneity of the IRONSperm can affect the electrostatic and magnetic interactions between the individual IRONSperm samples [8], but will not affect the magnetic properties of the IRONSperm cluster.

The size of a cluster mainly depends on the following properties: the concentration of cells and the concentration of the nanoparticles (NPs) attached. Furthermore, the preparation parameters such as the self-assembly time and the magnetic field strength influence the cluster size as well. A low concentration of IRONSperm means a greater distance between the cells. This results in the need for greater attractive forces, than when the distance between cells is smaller. These attractive forces can be increased by increasing the induced magnetic moment of the rotating magnetic field.

2.2.1 Step-out frequency of IRONSperm clusters

The step-out frequency is the frequency at which the entire available magnetic torque is required to maintain synchronous rotation[11]. Above this frequency, the magnetic torque is not strong enough to keep the cluster synchronized with the rotating magnetic field. The step-out frequency depends on the cluster's magnetization, friction and the rotating field strength. If the cluster is operated above the step-out frequency, the angular velocity declines.

A magnetic field exerts a torque on an IRONSperm cluster such that

$$\boldsymbol{\tau}_m = \mathbf{m} \times \mathbf{B}, \quad (1)$$

where τ_m is the magnetic torque, m is the magnetic moment, and B is the magnetic field strength. Apart from the magnetic torque, the viscous drag force and friction exert force on the IRONSperm cluster. The viscous drag force is defined as follows:

$$\boldsymbol{\tau}_d = f_r \boldsymbol{\omega}_c, \quad (2)$$

where f_r is the rotational drag coefficient of the cluster and $\boldsymbol{\omega}_c$ is the angular velocity, such that $\boldsymbol{\tau}_m + \boldsymbol{\tau}_d + \boldsymbol{\tau}_f = 0$. When the clusters fail to align their magnetic moment with the rotating magnetic field, they stop to rotate in uniform and the step-out frequency is reached. The formula for the angular velocity of the cluster, above the step-out frequency, is given by [8]

$$\omega_c = \frac{d\vartheta_c}{dt} = \omega_{so} \sin(\omega_f t - \vartheta_c), \quad (3)$$

with $\omega_{so}(\text{rad s}^{-1})$ as the step-out frequency, ω_f the angular velocity of the magnetic field, and time (t). Below the step-out frequency, the angular velocity of the cluster equals the angular velocity of the rotating magnetic field.

2.2.2 Neighboring forces on clusters

In a low Reynolds number with a solid boundary close to the IRONSperm cluster, the speed is dictated mainly by the magnetic force of the surrounding clusters, \mathbf{F}_m , the viscous drag force, \mathbf{F}_d and the frictional force \mathbf{F}_f such that $\mathbf{F}_d + \mathbf{F}_m + \mathbf{F}_f = 0$ [8]. With the formula for the viscous drag force as follows: $\mathbf{F}_d = -f_t \mathbf{v}$, with translational drag coefficient f_t and v the velocity of the cluster. The magnetic force that a cluster with magnetic moment \mathbf{m}_1 exerts on a neighboring cluster with a magnetic moment \mathbf{m}_2 is given by [8]:

$$\mathbf{F}_m = \frac{3\mu_0}{4\pi|\mathbf{r}|^4} (\mathbf{m}_2(\mathbf{m}_1 \cdot \hat{\mathbf{r}}) + \mathbf{m}_1(\mathbf{m}_2 \cdot \hat{\mathbf{r}}) + \hat{\mathbf{r}}(\mathbf{m}_1 \cdot \mathbf{m}_2) - 5\hat{\mathbf{r}}(\mathbf{m}_1 \cdot \hat{\mathbf{r}})(\mathbf{m}_2 \cdot \hat{\mathbf{r}}), \quad (4)$$

with $\hat{\mathbf{r}}$ as the unit vector between the clusters and $|\mathbf{r}|$ the distance between the two clusters, clarified in figure 1. Since the equation describes the forces between two clusters, this force is only a factor when two clusters are close together.

2.2.3 Rotation of clusters

When a rotating magnetic field activates the cluster, the magnetized parts on the IRONSperm start

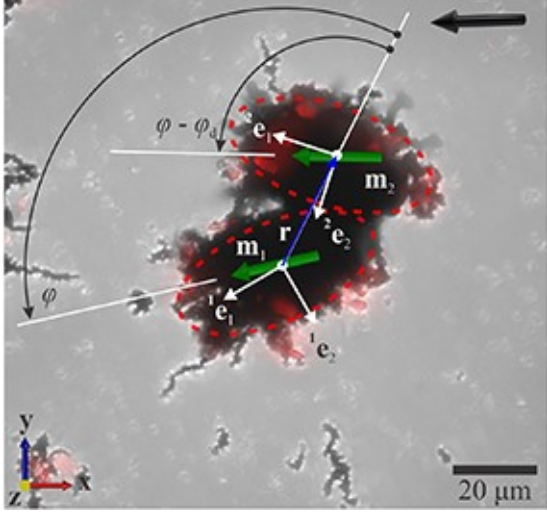


FIGURE 1: Two aggregate IRONSperm clusters in a rotating magnetic field, defining the parameters used in equation 4 [8].

to align themselves with the magnetic field. Since the cluster is heavily entangled, it acts as a single-body soft magnet [8]. The cluster trails behind the rotating magnetic field, aligning its magnetic moment with the magnetization axis of the field. When two clusters rotate synchronously, the attractive force between these two clusters is given by:

$$\frac{1}{2\pi} \int_0^{2\pi} \mathbf{F}_m \cdot (-\hat{\mathbf{r}}) d\varphi = \frac{3\mu_0 |\mathbf{m}_1| |\mathbf{m}_2|}{8\pi(|\mathbf{r}|)^4} \cos(\varphi_d), \quad (5)$$

With the forces per rotation. Where φ is the angle between \mathbf{r} and \mathbf{m}_1 , and φ_d is the angle between \mathbf{m}_1 and \mathbf{m}_2 , such that $-\pi/2 \leq \varphi_d \leq \pi/2$. This force is positive for all possible values of φ_d , causing the clusters to come together.

2.2.4 Rolling locomotion

The rotational motion of a cluster in a rotating magnetic field results in locomotion. In this case, the cluster is close to a solid boundary and rolling is the locomotion mechanism that will occur. When a cluster is in contact with a solid boundary, the application of an rotating magnetic field along the surface of the boundary causes the cluster to roll [8]. When a cluster starts rolling, it travels the distance of its perimeter during one rotation of the magnetic field, assuming no slipping takes place. This means that the velocity (v) of the cluster is linearly dependent on the perimeter (p) of the cluster and the rotating

magnetic field frequency (ω_f), such that

$$v = p\omega_f/(2\pi), \quad (6)$$

Rotation around the Y-axis gives a rolling motion in the X-axis. Rotation around the X-axis gives a rolling motion in the Y-axis.

2.2.5 Breaking down of the clusters

When rotating, several forces act on the body. When these forces become greater than the combination of the electrostatic, magnetic and entanglement forces, the cluster can break into smaller clusters. Centripetal and centrifugal forces are the forces experienced by rotating objects. Centripetal forces are the forces that are experienced by the body, that try to pull it towards the centre of rotation.

By Newton's second law, the cause of acceleration is a net force acting on the object, which is proportional to its mass m and its acceleration. The force, usually referred to as a centripetal force, has a magnitude

$$\mathbf{F}_c = m\mathbf{a}_c = m \frac{\mathbf{v}^2}{\mathbf{r}}, \quad (7)$$

and is, like centripetal acceleration, directed toward the center of curvature of the object's trajectory [12]. Where in this equation, r is any distance of the centre of the cluster to the desired point, and m is the mass of this point.

Furthermore, centrifugal forces also play a role in the cluster breaking down from rotational forces. Centrifugal forces are the apparent outward forces on a mass that is rotated [13]. This contributes to the following equation:

$$\mathbf{F} = m\omega^2\mathbf{r}, \quad (8)$$

with F the centrifugal force, m the mass, r the radius and ω the angular velocity of the cluster. When the clusters break apart, the centrifugal force is greater than centripetal, magnetic and entanglement forces combined.

2.2.6 Navigating the cluster

The cluster can only be directed in limited ways. Since the locomotion is controlled by a rotating magnetic field, the rotation of the end-effector will not influence the direction of the cluster. Furthermore,

the rotation of the end-effector perpendicular to the rolling motion only influences the rotation axis of the cluster. This results in the cluster's locomotion only being able to be controlled in one plane simultaneously.

3 Preparatory work

3.1 3D reconstruction of the phantom

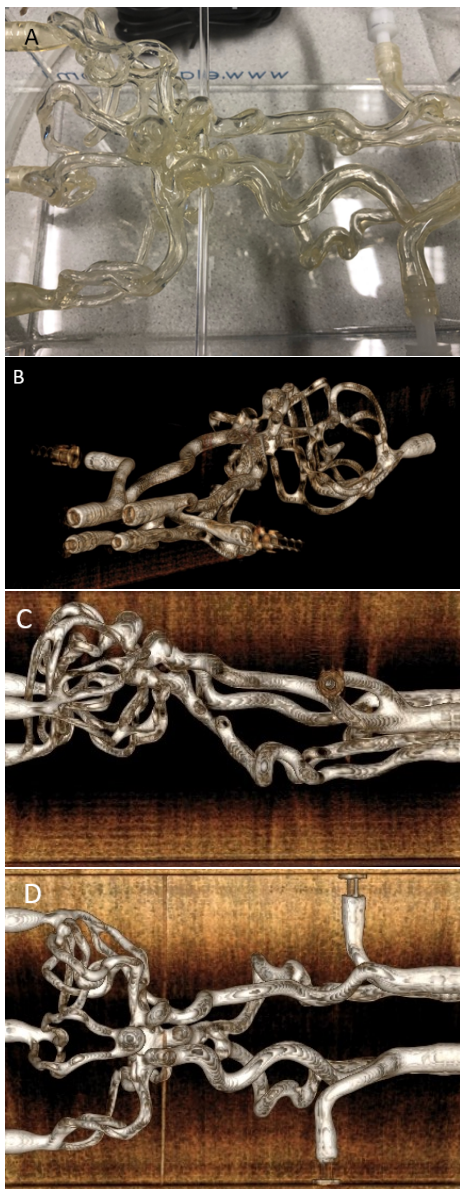


FIGURE 2: 3D reconstruction with the C-arm (figure 2B) of the vascular system phantom (figure 2A) by the C-arm, along with the side- (2 C) and topview (2D) of the phantom used for the centerline extraction.

3D reconstruction of the phantom is required to quantitatively determine the centerline. The reconstruction was done by the Siemens Artis Pheno C-arm, with a 7s scan time, 71kV tube voltage and 16mA tube current.

3.2 Centerline extraction

The top and side views of the 3d scan were used to extract the centerline (figure 2C-D). It was chosen to extract 26 waypoints over the phantom's track, each indicating a significant change in the orientation. From figure 2C, the y and z coordinates of these waypoints are determined, from figure 2D the x and y coordinates are determined. When connecting these coordinates, the waypoints in the 3D space yield the centerline of the phantom's track, shown in figure 3.

With these waypoints and the centerline, the tangent, normal and binormal vectors corresponding to the waypoints can be determined. The vectors are determined by the angle between the corresponding and following waypoint and the rotation matrix that describes the two points.

3.3 Setup

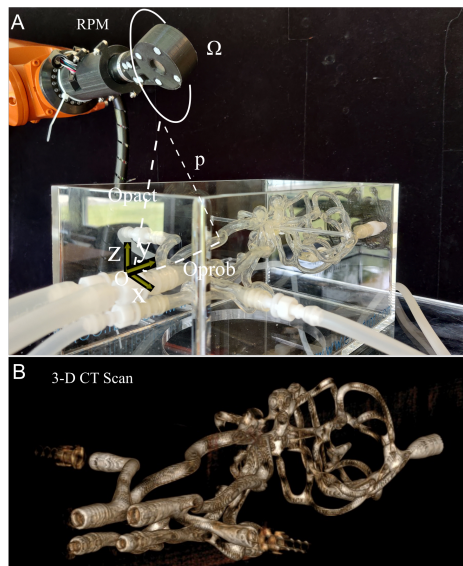


FIGURE 4: Visual representation of the setup. in figure 4A, the actuator with Ω as the rotation of the permanent magnet, $^o p_{act}$ the distance of the actuator to the origin, $^o p_{prob}$ the distance of the IRONSperm cluster to the origin and p the distance of the actuator to the cluster. Figure 4b visualizes the phantom from this point of view.

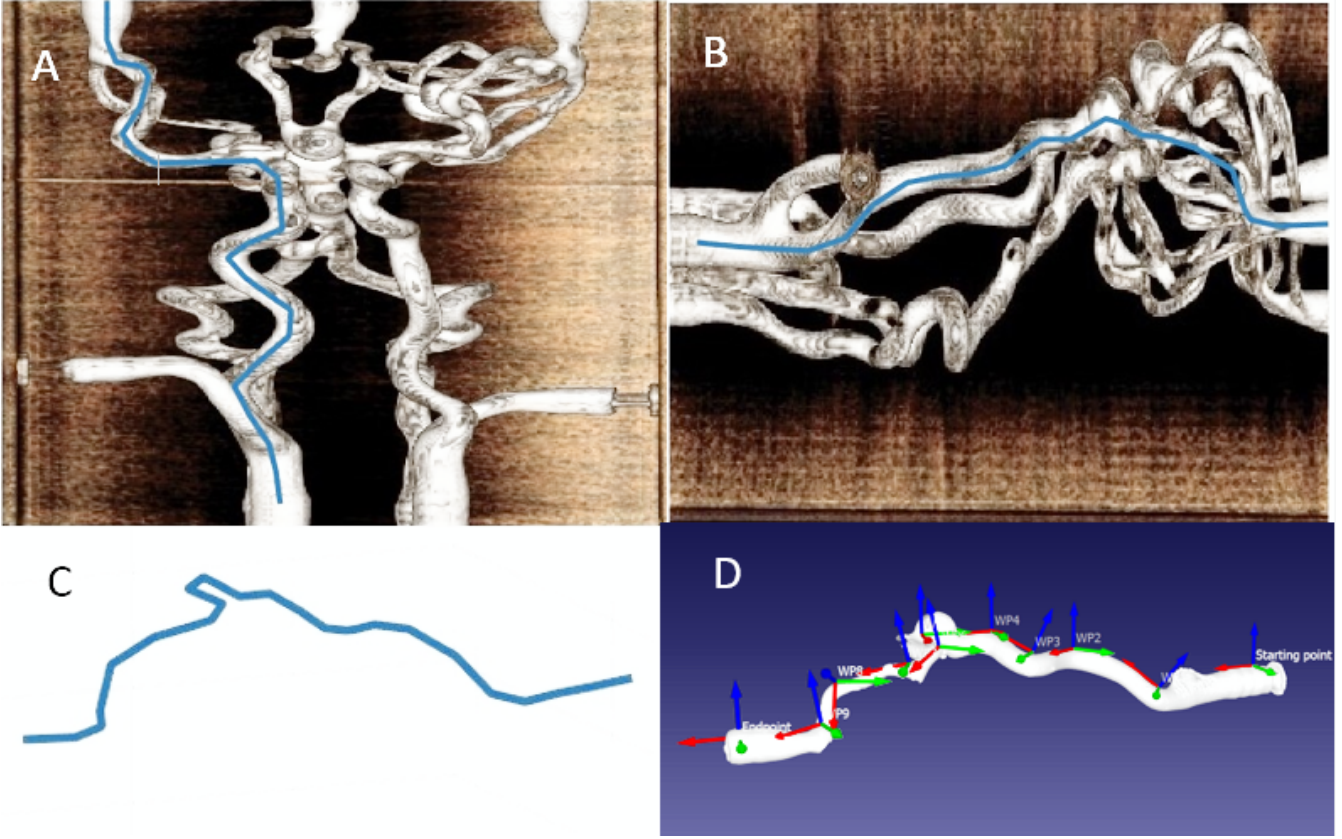


FIGURE 3: The reconstructed centerline of the phantom's track overlaid on the phantom's topview (figure 3A), the sideview (figure 3B) and seen as 3D image (figure 3C). Figure 3D shows the tangent (red), normal (blue) and binormal (green) vectors between the 26 waypoints, only showing vectors at the 10 most important waypoints to keep the picture clear.

4 Methods

4.1 IRONSperm characterization

The IRONSperm samples were prepared by using $8,288 \times 10^7$ cells/ml with 3mg/mL of Fe_3O_4 nanoparticles. The IRONSperm characterization was done in a 10mm diameter tube filled with water. The actuator was set perpendicular to the tube, so rolling on the bottom of the tube could take place. The magnetic field rotated at 0.2 Hz.

4.2 KUKA joint configuration

The KUKA joint configuration and the corresponding path were programmed using RoboDK software. Linear movement was used to transfer between the waypoints and corresponding actuator angle (in the x,y-plane), ensuring the exact tracing of the centerline.

4.3 Phantom experiments

The phantom was filled with water. The bottom of the phantom was set at 46cm of the base of the KUKA. The magnetic ball with a diameter of 5mm was inserted at the origin of the starting point (figure 3D) and held in place with a permanent magnet until the actuator reached the starting position and rotation of the magnetic field started.

5 Results

5.1 IRONSperm characterization

The IRONSperm characterization was done by the methods mentioned in 4.1

5.1.1 Actuation distance

At $p = 20$ cm, no motion of the IRONSperm cluster could be acknowledged. The rotating permanent

magnet was then slowly moved closer to the cluster, until movement of the cluster could be acknowledged. At $p = 9\text{cm}$, the cluster can be seen waving along with the magnetic field, but the field strength is not strong enough to detach the cluster from the bottom and let it roll. At $p = 7\text{cm}$, the cluster started rolling. $p = 7\text{cm}$ can thus be seen as the minimum actuation distance for a constant response of the IRONSperm cluster.

5.1.2 Speed

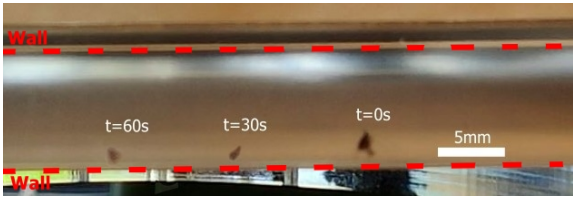


FIGURE 5: IRONSperm cluster actuated at a frequency of 0.2 Hz, while rolling in an H_2O filled tube of 10mm with the actuator at $p=7\text{cm}$.

With the actuation distance found, the speed of the cluster can be determined. The speed of the IRONSperm cluster was determined at a rotating magnetic field of 2Hz. The cluster was measured in time and distance while rolling in a straight line with the rotating magnetic field in a fixed position above the cluster. The speed was determined to be 0.32 mm/s, as can be deduced from figure 5.

5.1.3 Transfer distance

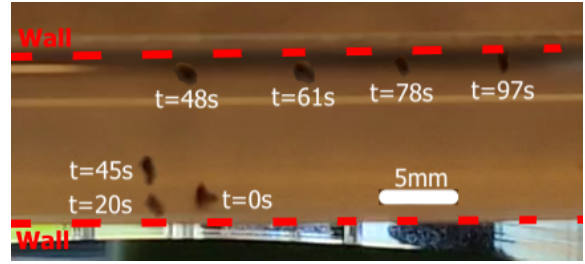


FIGURE 6: The cluster actuated at a frequency of 0.2 Hz in a tube of 10mm diameter. At $t=20\text{s}$, distance p was decreased from 7cm to 4.5cm over the span of 25s.

The cluster can be transferred from the bottom of the tube to the top and the other way around. By similar means to that of section 5.1.1, the distance p was decreased to 4.5cm, where the cluster started rising to the top of the tube. Once settled at the top, the speed of the cluster was compared to the speed of the cluster at the bottom of the tube as can be seen in figure 6.

5.2 IRONSperm proof of principle

To prove the principle of the mechanism, the rolling motion on top of the tube on an incline has to be tested.

As can be seen in figure 7, the IRONSperm cluster

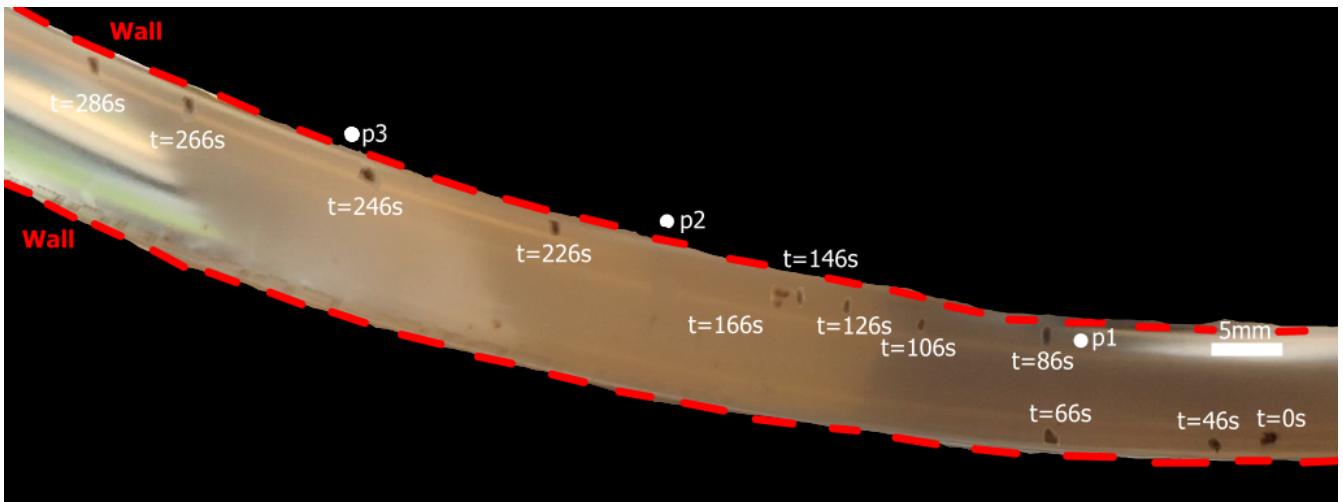


FIGURE 7: IRONSperm cluster actuated at 0.2 Hz with $p=7\text{cm}$ on an inclining surface in a tube with 10mm diameter. At $t=66\text{s}$, the cluster was stuck and thus p was decreased to 4.5cm. In order to keep the magnetic field strength strong enough, the position of the actuator was changed over time. at $t=0\text{s}$, the actuator was at p_1 , p_2 at $t=185\text{s}$ and p_3 at $t=268\text{s}$.

was rolling on the bottom until $t=66s$. At this point, p was decreased to 4.5cm to increase the magnetic field strength and attract the cluster to the top of the tube. This, including the decrease of p was done in a total of 20s. Afterwards, the cluster continued rolling upwards. Between $t=146s$ and $t=166s$, the cluster stopped rolling so the actuator was moved forward to $p2$. The cluster proved to be able to continue rolling upwards while the steepness increased up to $t=286s$.

5.3 KUKA joint configuration

The KUKA's (8) configuration is essential to navigate the cluster through the phantom. The bottom of the phantom's box is 46cm above the base of the KUKA. At every waypoint, the permanent magnet is set to aim at the next waypoint in the x,y -plane. When the centerline inclines, the cluster is transferred to the top of the tube. This requires the KUKA to decrease distance p . This leads to the following joint configuration, as can be seen in table 1.

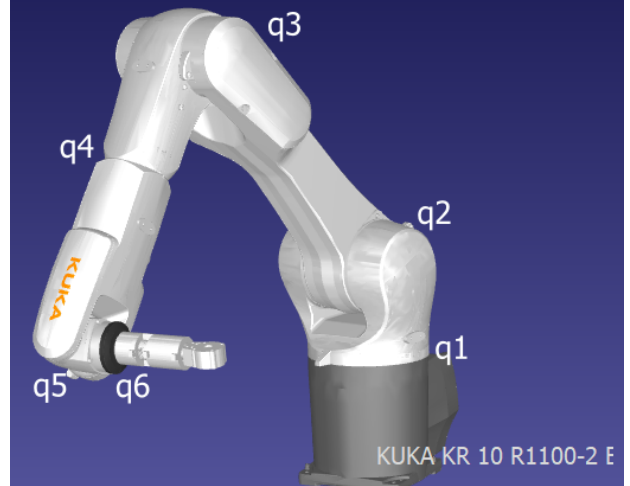


FIGURE 8: The KUKA KR 10 R1100-2 E used for the experimental setup, with the rotating magnet as the end-effector.

Waypoint	Joint 1 (deg)	Joint 2 (deg)	Joint 3 (deg)	Joint 4 (deg)	Joint 5 (deg)	Joint 6 (deg)
1	93.263	-84.849	132.730	4.395	-47.965	-2.946
2	90.821	-85.791	132.321	1.131	-46.536	-0.778
3	110.531	-66.817	108.122	91.384	-91.574	-48.676
4	99.738	-82.366	129.210	-141.309	53.801	154.686
5	83.782	-83.808	130.791	-20.523	-48.851	13.837
6	76.799	-81.708	128.874	-41.726	-55.318	26.904
7	96.246	-83.126	130.135	35.189	-52.697	-23.138
8	103.205	-77.708	123.280	63.840	-66.627	-38.925
9	105.532	-61.066	98.121	-78.907	104.294	128.450
10	105.058	-59.172	94.996	-79.513	104.150	-232.870
11	99.981	-77.240	122.235	55.226	-60.298	-35.512
12	84.418	-81.525	127.198	175.681	45.755	-176.984
13	83.159	-81.860	126.697	-5.420	-44.965	3.840
14	64.542	-68.219	108.103	97.375	81.266	229.551
15	65.844	-72.308	117.830	-68.441	-70.159	40.663
16	91.605	-78.582	127.110	-144.445	54.281	157.350
17	94.601	-77.762	122.897	-128.727	58.090	-213.389
18	94.567	-77.099	122.108	-127.314	58.784	-214.214
19	74.902	-79.511	125.327	-24.149	-48.431	16.567
20	63.241	-72.114	115.543	-68.248	-68.620	42.417
21	62.611	-73.769	117.342	-65.429	-66.391	41.216
22	79.812	-80.244	127.330	8.265	-47.385	-5.617
23	80.435	-79.738	126.170	15.006	-47.423	-10.279
24	72.841	-79.134	125.313	-12.913	-46.911	8.901
25	69.924	-78.400	124.280	-21.564	-47.953	14.825
26	66.434	-75.131	119.738	-32.775	-49.555	22.668

TABLE 1: All joint configurations (in deg) compliant with the waypoints extracted from figure 3

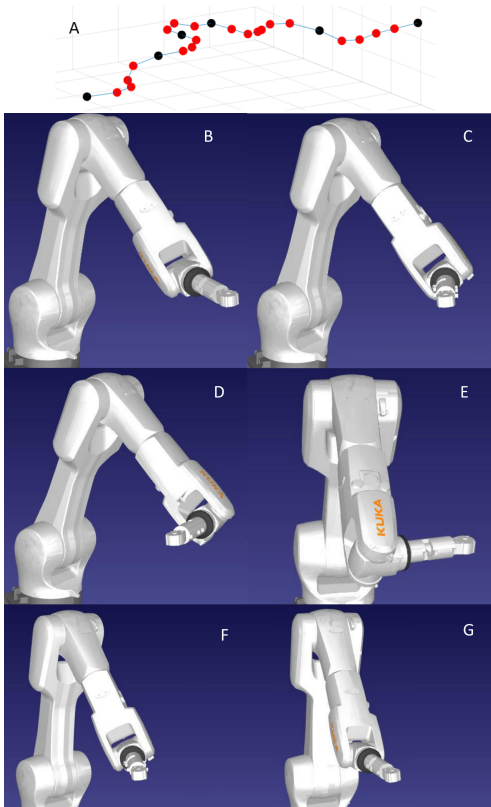


FIGURE 9: (A) The waypoints set for the KUKA, all on the centerline shown in figure 3C, starting with WP1 on the right, up to WP26 on the left. (B-G) The configuration of the KUKA is shown corresponding to the black waypoints highlighted in 9A, with B the right waypoint and G the left.

5.4 Phantom experiment IRONSperm cluster

With the joint configuration of table 1, navigation in the phantom was tried. First, p had to be decreased to 7cm when rolling on the bottom, and 4.5cm when rolling on the top. This proved to be impossible because the phantom's confinement collided with the actuator and restricted the KUKA's motion when set at this height. Due to these restrictions in distance p , the magnetic field was not strong enough to actuate the cluster and thus the experiment could not take place.

6 Discussion

6.1 IRONSperm samples

The IRONSperm samples were sent to us in a volume of 650 μL . This made it difficult to control the size of the IRONSperm cluster since the samples were clustered as one when arriving. This influences other properties such as the speed, step-out frequency and actuation distance as well. When actuating the samples from a close enough distance p (7cm or less), the samples responded well and gave a constant speed over a flat surface at a frequency of 0.2 Hz.

The initiation of the cluster's locomotion proved to be inconsistent at this distance p . The initial motion required a stronger magnetic field strength than when the locomotion had already started. This can be explained by the interactions of the IRONSperm with the surface of the tube, the natural surface properties of the IRONSperm, which tend to be attracted to boundaries [14].

6.2 Actuation distance

As said in 5.4, the actuation distance to the IRONSperm cluster was too small to properly experiment in the phantom. This is caused by a combination of the following: Nanoparticle concentration, the size of the IRONSperm cluster and magnetic field strength. The first two essentially come down to an increase in magnetic material in the cluster, increasing its magnetic moment and thus increasing the magnetic torque exerted on the IRONSperm cluster as can be seen in equation 1. According to the same equation, an increase in the magnetic field strength increases the magnetic torque on the cluster equally. This can be achieved by increasing the strength of the magnet that is located inside the end effector. In pursuit of a solution for this problem, a stronger magnet was placed in the end effector of the KUKA. This resulted in an increase of distance p for rolling to 8cm and transfer distance to 4.5cm. This did not solve the collision issue. It does prove, however, that when changing the magnetic field strength applied the actuation distance can be increased, and the KUKA gains more space to work with and is no longer obstructed by the phantom.

6.3 Recommendations

In future work, measurements in the phantom can give better insight into the behaviour of the IRONSperm cluster inside the human body. If the actuation distance can be increased and consequently the desired path can properly be followed, all the challenges of the phantom can be examined. One of the most interesting things to examine is the behaviour of the cluster in the smaller vessels since confinement on both sides of the cluster might influence the rolling motion since the same actuator rotation makes the cluster roll forwards or backwards depending on the reference on the top or bottom of the tube. Besides this, actuation of the IRONSperm cluster at higher frequencies can be investigated, to increase the speed and determine the influence of this on the breakdown of the cluster when moving through the phantom. Further experiments must thus be conducted where the restricting factors are minimized and the true behaviour of the cluster inside the phantom can be examined.

7 Conclusion

This paper investigated the control of an IRONSperm cluster in a phantom, modelled after the blood vessels in the neck and brain. First of all, the relevant motion control was tested in a tube. These tests proved that a cluster could roll, transfer from bottom to top and continue rolling in a tube. Furthermore, the control of a cluster on an inclining surface was tested. These tests proved to be successful and have great promise for the future. By a combination of these results, it should be possible to navigate the cluster in the phantom.

References

- [1] H. S. HIMAL. “Minimally invasive (laparoscopic) surgery”. In: *Surg. Endosc.* 16.12 (Dec. 2002), pp. 1647–1652. ISSN: 1432-2218. DOI: 10.1007/s00464-001-8275-7.
- [2] *Magnetically actuated microrobots as a platform for stem cell transplantation*. [Online; accessed 22. Jun. 2023]. June 2023. DOI: 10.1126/scirobotics.aav4317.
- [3] Zhengxin Yang and Li Zhang. “Magnetic Actuation Systems for Miniature Robots: A Review”. In: *Adv. Intell. Syst.* 2.9 (Sept. 2020), p. 2000082. ISSN: 2640-4567. DOI: 10.1002/aisy.202000082.
- [4] Metin Sitti and Diederik S. Wiersma. “Pros and Cons: Magnetic versus Optical Microrobots”. In: *Adv. Mater.* 32.20 (May 2020), p. 1906766. ISSN: 0935-9648. DOI: 10.1002/adma.201906766.
- [5] Morgan M. Stanton et al. “Biohybrid Janus Motors Driven by *Escherichia coli*”. In: *Adv. Mater. Interfaces* 3.2 (Jan. 2016), p. 1500505. ISSN: 2196-7350. DOI: 10.1002/admi.201500505.
- [6] Hakan Ceylan et al. “Translational prospects of untethered medical microrobots”. In: *Prog. Biomed. Eng.* 1.1 (July 2019), p. 012002. ISSN: 2516-1091. DOI: 10.1088/2516-1091/ab22d5.
- [7] Metin Sitti et al. “Biomedical Applications of Untethered Mobile Milli/Microrobots”. In: *Proceedings of the IEEE. Institute of Electrical and Electronics Engineers* 103.2 (Feb. 2015), p. 205. DOI: 10.1109/JPROC.2014.2385105.
- [8] Kaz I. N. A. Middelhoek et al. “Drug-Loaded IRONSperm clusters: modeling, wireless actuation, and ultrasound imaging”. In: *Biomed. Mater.* 17.6 (Sept. 2022), p. 065001. ISSN: 1748-605X. DOI: 10.1088/1748-605X/ac8b4b.
- [9] Veronika Magdanz et al. “IRONSperm: Sperm-templated soft magnetic microrobots”. In: *Sci. Adv.* 6.28 (July 2020). DOI: 10.1126/sciadv.aba5855.
- [10] Veronika Magdanz et al. “Impact of Segmented Magnetization on the Flagellar Propulsion of Sperm-Templated Microrobots”. In: *Adv. Sci.* 8.8 (Apr. 2021), p. 2004037. ISSN: 2198-3844. DOI: 10.1002/adv.202004037.
- [11] Arthur W. Mahoney et al. “Behavior of rotating magnetic microrobots above the step-out frequency with application to control of multi-microrobot systems”. In: *Appl. Phys. Lett.* 104.14 (Apr. 2014). ISSN: 0003-6951. DOI: 10.1063/1.4870768.
- [12] Tilman Spohn, Doris Breuer, and Torrence V. Johnson. *Encyclopedia of the Solar System*. Waltham, MA, USA: Elsevier, 2014. ISBN: 978-0-12-415845-0. DOI: 10.1016/C2010-0-67309-3.
- [13] *Centrifugal Force - an overview | ScienceDirect Topics*. [Online; accessed 7. Jun. 2023]. June 2023. DOI: 10.1016/B978-0-323-95717-5.00020-7.
- [14] Jens Elgeti, U. Benjamin Kaupp, and Gerhard Gompper. “Hydrodynamics of Sperm Cells near Surfaces”. In: *Biophys. J.* 99.4 (Aug. 2010), p. 1018. DOI: 10.1016/j.bpj.2010.05.015.

A Appendix

A.1 Phantom experiment permanent magnet

With the KUKA configuration, tests were done with a permanent magnet instead of an IRONSperm cluster to test the configuration. The speed of the permanent magnet was determined to be 5.9mm/s.

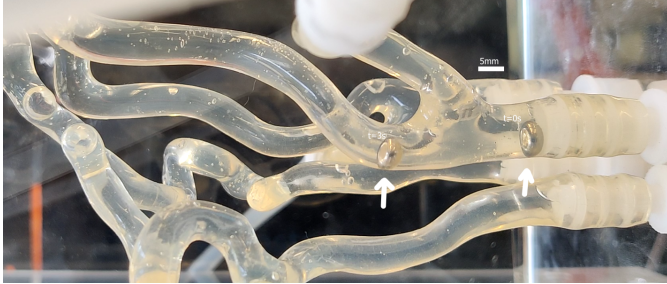


FIGURE 10: Permanent magnetic ball of 5mm diameter in the phantom while the actuator follows the centerline path. At $t=0s$ (on the right), the rotating field was applied, whereafter a rolling motion was observed. After $t=6s$, the ball kept rolling but no significant change in position was observed for the following 60 seconds.

As can be seen in figure 10, the permanent magnet did not behave as expected. First of all, when looking at the distance travelled between $t=0s$ and $t=3s$, the distance that the magnetic ball had rolled was significantly higher than the expected distance (around 25mm instead of the expected 17.7mm). After 3 seconds, the ball could still be seen rotating but slipping made sure the ball could not move over the inclining path. When moving the rotating magnet closer to transfer the ball to the top of the centerline, the magnetic attractive forces overruled the rotating magnetic field, and no movement of the ball could be acknowledged anymore.